Modeling of Solid–Liquid Equilibria for Polyethylene and Polypropylene Solutions with Equations of State

G. M. N. Costa,[1] S. Kislansky,[1] L. C. Oliveira,[1] F. L. P. Pessoa,[2] S. A. B. Vieira de Melo,[1] M. Embiruçu[1]

[1]*Programa de Engenharia Industrial, Escola Politécnica, Universidade Federal da Bahia, Rua Professor Aristides Novis, 2, Federação, CEP 40210-630, Salvador-Bahia, Brazil*
[2]*Departamento de Engenharia Química, Escola de Química, Universidade Federal do Rio de Janeiro, Centro de Tecnologia, bloco E, S. 209, Ilha do Fundão, 21949-900, Rio de Janeiro RJ, Brazil*

Received 9 May 2010; accepted 4 August 2010
DOI 10.1002/app.33128
Published online 10 March 2011 in Wiley Online Library (wileyonlinelibrary.com).

ABSTRACT: We modeled solid–liquid equilibria (SLEs) in polyethylene and polypropylene solutions with a Soave–Redlich–Kwong (SRK) cubic equation of state (EOS) and a perturbed-chain statistical associating fluid theory (PC-SAFT) EOS. Two types of mixing rules were used with SRK EOS: The Wong–Sandler mixing rule and the linear combination of the Vidal and Michelsen mixing rules (LCVM), both of which incorporated the Bogdanic and Vidal activity coefficient model. The performance of these models was evaluated with atmospheric-pressure and high-pressure experimental SLE data obtained from literature. The basic SLE equation was solved for the equilibrium melting temperature instead of for the composition. The binary interaction parameters of SRK and PC-SAFT EOS were estimated to best describe the experimental equilibrium behavior of 20 different polymer–solvent systems at atmospheric pressure and 31 other polymer–solvent systems at high pressure. A comparison with experimental data showed that SRK–LCVM agreed very well with the atmospheric SLE data and that PC-SAFT EOS was more efficient in high-pressure conditions. © 2011 Wiley Periodicals, Inc. J Appl Polym Sci 121: 1832–1849, 2011

Key words: phase behavior; phase diagrams; phase separation; poly(propylene); (PP); polyethylene (PE)

INTRODUCTION

Polyethylene (PE) and polypropylene (PP) are global commodity polymers. During the industrial processing of PE and PP, deposition of the polymer on the reactor surface, heat exchangers, and flash drums frequently occurs, and in pipelines, this can cause clogging. Therefore, the solubility behavior of the polymer is key information for solvent selection and polymer processing in industry. For instance, in the solution polymerization of ethylene, the PE produced in the reactors should remain in solution because its precipitation from the solution is undesirable.[1–3] Solvent selection is also crucial and is dependent on the polymer solubility because polymer recycling requires detailed screening and identification of possible solvents for the polymers in the waste material.[4] The modeling of solid–liquid equilibrium (SLE) is a useful method for gaining a better understanding of these industrial polymer problems and, thus, stop them from occurring, a task that cannot be done with empirical models,[5] especially when one is dealing with complex systems, such as solution and slurry polymerization reactions.[6,7]

Two basic approaches can be used to model the liquid-phase nonideality in SLE: excess Gibbs free-energy (G^E) models and equations of state (EOSs). Some researchers have attempted to describe the liquid-phase nonidealities using the universal quasi-chemical (UNIQUAC) functional-group activity coefficient and entropic free volume (entr-FV) models[4] or by applying perturbed-chain statistical associating fluid theory (PC-SAFT) EOS to the modeling of SLE of binary and ternary systems with a solid-complex phase formation.[8] Some work has also been done on the development of algorithms for the real-time prediction of SLE in the solution polymerization of PE based on PC-SAFT EOS and to study the effects of monomer and polymer polydispersity in solution polymerization processes.[9] Furthermore, copolymer PC-SAFT EOS have been used to model SLE in systems containing PE, *m*-xylene, and amyl acetate.[10]

Polymer solutions are not adequately described by cubic EOSs and their van der Waals type one-fluid mixing rules. However, over the past 2 decades, a large number of mixing rules have been proposed to improve the performance of these kinds of equations

Correspondence to: M. Embiruçu (embirucu@ufba.br).
Contract grant sponsors: Fundação de Amparo à Pesquisa do Estado da Bahia, Conselho Nacional de Desenvolvimento Científico e Tecnológico.

in representing the phase behavior for highly nonideal mixtures, such as PE and PP solutions.[6,11] Mixing rules for cubic EOSs derived from G^E models, called EOS/G^E models, such as the linear combination of the Vidal and Michelsen mixing rules (LCVM)[12] and the Wong–Sandler (WS)[13] mixing rule, have been proposed extensively for the prediction of vapor–liquid equilibrium, but they are rarely used to describe SLE behavior.

In this study, only the EOS approach was used to investigate the liquid-phase nonideality in SLE for polymer systems. PC-SAFT and Soave–Redlich–Kwong (SRK)[14] EOS were chosen, with LCVM and WS mixing rules. On the basis of a previous article, in which the evaluation of several activity coefficient models, both at infinite dilution and finite concentration, were reported, the Bogdanic and Vidal (BV) activity coefficient model was selected to be incorporated into LCVM and WS mixing rules of the SRK EOS.[15]

These three EOS-based models (PC-SAFT, SRK–WS, and SRK–LCVM) were used to solve the equilibrium equation for temperature. Experimental atmospheric (for both nonassociated and associated systems) and high-pressure SLE data available in the literature were used to compare their performances. The Newton–Raphson (NR) and Regula–falsi (Rf) numerical methods[16–19] were used and compared to solve this equilibrium equation. For both atmospheric and high-pressure experimental data, the performances of the models with the estimated interaction parameters averaged over all temperatures were investigated, and the feasibility of obtaining generalized correlations among the binary interaction parameters and the independent variables, such as polymer molecular weight (MW) and polymer concentration, was evaluated. Finally, for high-pressure conditions, the influence of the solvent, pressure range, and polymer MW on the performance of the models and the parameter correlation interpolating and extrapolating capabilities were examined through the charting of the experimental and model results.

THERMODYNAMIC MODELS

Solubility basic equation

Following the hypothesis of Harismiadis and Tassios[4] about the fugacity ratio and its relationship with crystallinity, Pan and Radoz[10] assumed the solid phase to be pure solute and ignored the two heat-capacity terms, proposing a SLE model on the basis of an EOS, which is given as follows:

$$\ln\left(\frac{\varphi_p^L x_p}{\varphi_p^0}\right) = -\left(\frac{\Delta H_u}{RT_m}\times\left(\frac{T_m}{T}-1\right)+\frac{\Delta vP}{RT}\right)\times cu \quad (1)$$

where ϕ is the fugacity coefficient, the subscript p stands for the polymer (solute), the superscript L stands for the polymer in solution, the superscript 0 refers to the pure liquid polymer, x is the molar fraction (solubility) in solution, ΔH_u is the enthalpy of melting per moles of crystal units, R is the gas constant, T_m is the polymer melting temperature, T is the temperature, Δv is the polymer volume change, P is the pressure, c is the crystallinity fraction, and u is the number of monomer units in the polymer backbone. The ϕ values are calculated by an EOS.

PC-SAFT EOS

The PC-SAFT EOS is based on a perturbation theory, where the hard-chain reference term represents the repulsive forces and the perturbation terms reflect the various attractive interactions, as described in detail elsewhere.[20,21] To associate fluids, this EOS is conveniently written in terms of the reduced residual Helmholtz free energy as follows:

$$\frac{A^{\text{res}}}{NkT} = \frac{A^{hc}}{NkT} + \frac{A^{\text{disp}}}{NkT} + \frac{A^{\text{assoc}}}{NkT} \quad (2)$$

where A is the Helmholtz free energy per number of molecules, where the superscripts res, hc, disp, and assoc identify the residual, hard-chain, dispersive attraction, and associative attraction contributions, respectively; N is the total number of molecules; and k is the Boltzmann constant. The three terms on the right-hand side of eq. (2) correspond to the hard-chain, dispersion, and association contributions, respectively. All of the required expressions for these terms in eq. (2) and the pure-component parameters for many substances can be found in the literature.[20,21] When PC-SAFT is used for mixtures, the conventional Berthelot–Lorenz combining rules used to calculate the mixture properties in the hard chain and the dispersion term are applied, with only one adjustable binary interaction parameter of the PC-SAFT EOS (K_{ij}) introduced to account for the dispersive interactions, as follows:

$$\sigma_{ij} = \frac{1}{2}(\sigma_i + \sigma_j) \quad (3)$$

$$\varepsilon_{ij} = \sqrt{\varepsilon_i \varepsilon_j}\times(1 - K_{ij}) \quad (4)$$

where σ is the segment diameter, ε is the dispersion energy parameter, and the subscripts i and j refer to specific components or groups.

SRK EOS

The SRK EOS[14] is expressed as follows:

$$P = \frac{RT}{v-b} - \frac{a(T)}{v(v+b)} \quad (5)$$

where a and b are parameter of the SRK EOS. To extend the SRK EOS to polymer–solvent systems, the following mixing rules were considered: WS and LCVM.

WS mixing rule

The WS mixing rule[13] is a representative rule based on the condition of infinite pressure, given as follows:

$$a = b\sum_i \frac{x_i a_i}{b_i} + \frac{G^E}{d} \tag{6}$$

$$b = \frac{\sum_i \sum_j x_i x_j [b - a/(RT)]_{ij}}{1 - \sum_i x_i [a_i/(b_i RT)] - [G^E/dRT]} \tag{7}$$

with

$$\left(b - \frac{a}{RT}\right)_{ij} = \frac{1}{2}\left[\left(b - \frac{a}{RT}\right)_i + \left(b - \frac{a}{RT}\right)_j\right](1 - \mathrm{WS_{ij}}) \tag{8}$$

where d is a numerical constant equal to $(-\ln 2)$ for the SRK EOS and WS_{ij} is the binary interaction parameter.

LCVM mixing rule

Boukouvalas et al.[12] proposed the LCVM mixing rule as follows:

$$\alpha = \frac{a}{bRT} = \left[\sum x_i \alpha_i\right] + \left[\left(\frac{\lambda}{A_v} + \frac{1-\lambda}{A_M}\right)\frac{G^E}{RT}\right] + \left[\frac{1-\lambda}{A_M}\sum x_i \times \ln\left(\frac{b}{b_i}\right)\right] \tag{9}$$

where $A_v = -\ln 2$ and $A_M = -0.53$ for the SRK EOS and $\lambda = 0.36$, as originally proposed by Boukouvalas et al[12]. The conventional linear mixing rule is used for parameter b.

G^E model

Both the LCVM and WS mixing rules require a G^E model, and as mentioned previously, the BV[22] model is the best choice.[15] BV is a segment-based model containing combinatorial, free volume (FV), and energy contributions for G^E. It is derived from the entr-FV model and follows the idea of relating the nonideality of polymer–solvent mixtures with the polymer segment–solvent interaction parameters. The energetics contribution is based on interactions among individual segments (repeating units) of the polymer (or copolymer) and solvent molecules. The segment activity coefficients are calculated through the UNIQUAC model.

The molar activity coefficient of component i (γ_i) in the mixture is given by

$$\ln \gamma_i = \ln \gamma_i^{\mathrm{entr-FV}} + \ln \gamma_i^{\mathrm{res}} \tag{10}$$

where the first term on the right-hand side of eq. (10) represents the entr-FV contribution and the second one is the residual contribution.

As in the original model, the combinatorial and FV contributions are combined in a single term, the so-called entr-FV part:

$$\ln \gamma_i^{\mathrm{entr-FV}} = \ln\left(\frac{\beta_i^{\mathrm{FV}}}{x_i}\right) + 1 - \frac{\beta_i^{\mathrm{FV}}}{x_i} \tag{11}$$

where β_i^{FV} and x_i are the free-volume fraction and the molar fraction of the segment, respectively. FV is defined as

$$v_{\mathrm{FV},i} = v_i - v_{W,i} \tag{12}$$

where v_i and $v_{W,i}$ are the liquid molar volume and the van der Waals volume, respectively.

For the calculation of the residual term ($\ln \gamma_i^{\mathrm{res}}$), the mixture is considered a solution of segments and the molar fraction of each segment (X) is calculated by:

$$x_k = \frac{\sum_i^{\mathrm{ncomp}} x_i \delta_k^{(i)}}{\sum_j^{\mathrm{ncomp}} \sum_m^{\mathrm{nseg}} x_j \delta_m^{(j)}} \tag{13}$$

where x is the component (i or j) molar fraction, the subscripts k and m refer to segments and δ refers to the number of segments in a component (i or j). The summations are extended to the total number of components (*ncomp*) and to the total number of segments (*nseg*). The segment activity coefficients are calculated with the UNIQUAC model, which contains an interaction parameter denoted as UQ_{ij}.

EXPERIMENTAL DATA AND GENERAL APPROACH FOR CALCULATING SLE

Experimental data

Although the crystallization of polymer solutions has received much attention recently, most studies have focused on the kinetics of the process and on the morphology of the crystals. Equilibrium data of solid polymer solutions are often scarce.

Experimental SLE data at atmospheric pressure available in the literature are presented in this article as temperature versus polymer solubility, and only those systems that presented a continuous SLE curve were selected. Tables I and II show the database for the 20 systems investigated with the temperature interval covering the whole range of weight fractions.

TABLE I
Data Points Contained in the Database Used for the Solid–Liquid Calculations at Atmospheric Pressure: Nonassociated Systems

System	Number of data points	Temperature range (K)	Reference
1. PE (17,000)/xylene	8	345–376	23
2. PE (13,600)/heptane	5	341–351	23
3. PE (20,000)/dyphenil	6	377–383	24
4. PP (243,000)/tetradecane	3	435–452	25
5. PP (243,000)/eicosane	3	445–455	25
6. PP (28,000)/*n*-octane	3	331–357	26
7. PP (28,000)/*cis*-decalin	3	321–348	26
8. PE (13,600)/cetene	7	356–362	23
9. PE (31,000)/xylene	6	370–380	27
10. PE (32,600)/xylene	6	376–384	27
11. PE (13,600)/paraffin wax	7	357–370	23

TABLE II
Data Points Contained in the Database Used for the Solid–Liquid Calculations at Atmospheric Pressure: Associated Systems

System	Number of data points	Temperature range (K)	Reference
12. PP (243,000)/$C_{32}H_{66}$	3	446–456	25
13. PP (28,000)/*n*-amyl alcohol	4	371–384	26
14. PP (28,000)/*n*-hexyl alcohol	4	360–382	26
15. PP (28,000)/*n*-octyl alcohol	4	369–382	26
16. PP (28,000)/ isoamylacetate	4	357–368	26
17. PP (28,000)/phenetol	4	357–368	26
18. PP (28,000)/anisole	4	358–366	26
19. PP (243,000)/ *n*-eicosanoic	3	443–453	25
20. PP (243,000)/ *n*-pentadecanoic	3	444–454	25

The high-pressure SLE experimental data are shown in Tables III and IV with the corresponding polymer concentrations, pressures, and temperature ranges. The selected solvents at these pressures and temperatures were in a supercritical state.

Polymer properties for thermodynamic models

The polymer properties used in eq. (1), such as ΔH_u and polymer T_m, were obtained from van Krevelen.[31]

Δv was determined from the densities of an amorphous polymer (ρ_a) and a crystalline one (ρ_c): $\Delta v = 1/\rho_a - 1/\rho_c$. For PE, $\rho_a = 0.853$ g/cm^3 and $\rho_c = 1.004$ g/cm^3.[10] u was calculated with the polymer and monomer MWs. Although c of the polymer could have been used as an adjusted parameter, we

TABLE III
Data Points Contained in the Database Used for the Solid–Liquid Calculations at High Pressure

System	Polymer concentration	Number of data points	Pressure range (atm)	Temperature range (K)	Reference
21. PE (7000)/ethane	2.00	6	808–1501	372–381	28
22. PE (7000)/ethane	20.00	5	902–1503	375–383	28
23. PE (23,625)/ethane	2.00	4	1205–1509	372–377	28
24. PE (23,625)/ethane	20.00	4	1206–1511	372–378	28
25. PE (52,000)/ethane	20.00	4	1208–1513	399–403	28
26. PE (7000)/propane	2.00	6	605–1509	364–371	28
27. PE (7000)/propane	2.70	6	401–1502	364–372	28
28. PE (7000)/propane	7.40	6	597–1502	365–375	28
29. PE (7000)/propane	17.50	5	503–1502	366–378	28
30. PE (13,600)/propane	0.25	3	448–587	383–384	29
31. PE (13,600)/propane	2.00	3	550–688	387	29
32. PE (13,600)/propane	5.00	4	520–725	387–388	29
33. PE (13,600)/propane	10.00	4	475–656	387–388	29
34. PE (23,625)/propane	2.00	5	397–1500	365–372	28
35. PE (23,625)/propane	6.90	6	804–1500	366–374	28
36. PE (23,625)/propane	17.00	11	704–1510	366–376	28
37. PE (42,900)/propane	0.06	3	616–686	382–383	29
38. PE (42,900)/propane	3.00	4	628–702	387	29
39. PE (52,000)/propane	2.00	6	804–1513	394–404	28
40. PE (52,000)/propane	7.30	5	667–1508	393–405	28
41. PE (52,000)/propane	17.00	5	705–1513	393–405	28
42. PE (59,300)/propane	2.00	11	804–1500	389–395	28
43. PE (119,600)/propane	7.50	3	667–735	391–392	29
44. PE (121,000)/pentane	5.00	17	81–537	371–374	30
45. PE (7000)/ethylene	2.00	4	1200–1501	378–383	28
46. PE (23,625)/ethylene	2.00	4	1702–1969	380–382	28

TABLE IV
Data Points Contained in the Database Used to Test the Correlations for the Solid–Liquid Calculations at High Pressure

System	Polymer concentration	Number of data points	Pressure range (atm)	Temperature range (K)	Reference
47. PE (23,625)/propane	1.90	4	911–1504	369–380	28
48. PE (42,900)/propane	1.00	2	688–721	385	29
49. PE (52,000)/propane	1.90	5	705–1503	393–404	28
50. PE (119,600)/propane	0.25	2	609–613	388–389	29
51. PE (119,600)/propane	3.50	2	652–687	389–390	29

used the values reported with the experimental data or, when these were missing, the values assumed by Harismiadis and Tassios.[4]

As mentioned previously, three EOS were used to calculate ϕ_p^L and ϕ_p^0: PC-SAFT, SRK–LCVM, and SRK–WS. Calculations with the SRK EOS require pure component parameters, which use critical data as input for their computation; however, for polymers, these critical data are not available. Therefore, in this study, the pure polymer parameters were determined with Kontogeorgis et al.'s method.[32] According to this method, the polymer parameters a and b are fitted to two experimental volumetric data at essentially zero pressure. However, in this study, these parameters were obtained with the group contribution method group contribution volume (GCVOL)[33] because no experimental volumetric data were available. van der Waals volume data were taken from Bondi.[34]

GCVOL is a group contribution method for the prediction of the liquid densities for solvents, oligomers, and polymers as a function of temperature. Elbro et al.[33] proposed the following model for predicting the molar volume (v) of a liquid:

$$v = \sum n_i \Delta v_i \tag{14}$$

where n_i is the number of group i in the GCVOL method and the temperature dependence of the molar group Δv_i is given by the following simple polynomial function (the group volume temperature constants, A_i, B_i, and C_i, were available for 36 different groups):[33]

$$\Delta v_i = A_i + B_i T + C_i T^2 \tag{15}$$

As the SRK EOS polymer parameters a and b are functions of MW and temperature, different values of a and b for various values of these two properties could be calculated with the PE monomer constants: $A_i = 12.520$ cm^3/mol, $B_i = 0.01294$ cm^3 mol^{-1} K^{-1}, and $C_i = 0.0$ cm^3 mol^{-1} K^{-2}.

Numerical solution procedure

Solving eq. (1) for the solubility of the polymer is often a very hard task because of the instability of the numerical procedure.[4] To overcome this problem and to avoid multiple solutions, eq. (1) should be solved for temperature and not for composition. The Rf and NR methods[16–19] were used to find the root of this equation.

When the Rf and NR methods were applied for the first 11 nonassociated systems at atmospheric

TABLE V
Average and Maximum Percentile Temperature Errors for the Nonassociated Systems in the SLE at Atmospheric Pressure

	PC-SAFT			SRK–LCVM			SRK–WS		
System	AAD (%)	AMD (%)	Method	AAD (%)	AMD (%)	Method	AAD (%)	AMD (%)	Method
1	3.90×10^{-4}	4.66×10^{-1}	NR	3.69×10^{-4}	5.05×10^{-1}	NR	2.86×10^{-2}	1.01	Rf
2	3.25×10^{-4}	3.92×10^{-1}	NR	4.03×10^{-4}	5.79×10^{-1}	NR	4.45×10^{-4}	5.72×10^{-1}	NR
3	4.15×10^{-4}	6.14×10^{-1}	NR	3.97×10^{-4}	4.94×10^{-1}	NR	3.42×10^{-4}	3.91×10^{-1}	NR
4	7.39×10^{-2}	2.21×10^{-1}	NR	3.42×10^{-4}	3.79×10^{-1}	NR	5.56×10^{-4}	1.11	Rf
5	7.48×10^{-1}	2.24	NR	2.42×10^{-4}	2.70×10^{-1}	NR	3.32×10^{-4}	4.58×10^{-1}	NR
6	5.97×10^{-4}	8.49×10^{-1}	NR	4.30×10^{-4}	5.13×10^{-1}	NR	3.41×10^{-4}	4.27×10^{-1}	NR
7	3.19×10^{-2}	9.38×10^{-2}	NR	4.62×10^{-4}	4.98×10^{-1}	NR	3.98×10^{-4}	5.55×10^{-1}	NR
8	4.18×10^{-4}	5.61×10^{-1}	NR	3.74×10^{-4}	4.84×10^{-1}	NR	4.09×10^{-4}	5.85×10^{-1}	NR
9	1.15×10^{-3}	2.12×10^{-3}	NR	3.79×10^{-4}	4.66×10^{-1}	NR	5.76×10^{-2}	3.42×10^{-1}	Rf
10	1.47×10^{-3}	4.11×10^{-3}	NR	3.76×10^{-4}	4.17×10^{-1}	NR	3.89×10^{-4}	4.96×10^{-1}	Rf
11	6.80×10^{-4}	1.16	NR	3.89×10^{-4}	4.89×10^{-1}	NR	4.81×10^{-4}	6.24×10^{-1}	NR

AMD = max[($|T_i^{cal} - T_i^{exp}|/T^{exp}$) × 100], where $i = 1, N$; AAD = $(1/N) \times \Sigma(|T^{cal} - T^{exp}|/T^{exp}) \times 100$.

TABLE VI
Average and Maximum Percentile Temperature Errors for the Associated Systems in SLE at Atmospheric Pressure

	SRK–LCVM			SRK–WS		
System	AAD (%)	AMD (%)	Method	AAD (%)	AMD (%)	Method
12	2.55×10^{-4}	2.94×10^{-1}	NR	3.38×10^{-4}	3.66×10^{-1}	NR
13	2.35×10^{-4}	3.55×10^{-1}	NR	3.46×10^{-4}	3.87×10^{-1}	NR
14	3.30×10^{-4}	4.05×10^{-1}	NR	3.64×10^{-4}	3.98×10^{-1}	NR
15	3.69×10^{-4}	5.04×10^{-1}	NR	3.19×10^{-4}	3.73×10^{-1}	NR
16	3.34×10^{-4}	3.90×10^{-1}	NR	4.24×10^{-4}	5.70×10^{-1}	NR
17	3.20×10^{-4}	3.67×10^{-1}	NR	3.27×10^{-4}	4.18×10^{-1}	NR
18	3.32×10^{-4}	4.69×10^{-1}	NR	3.52×10^{-4}	4.11×10^{-1}	NR
19	3.07×10^{-4}	3.60×10^{-1}	NR	2.98×10^{-4}	3.33×10^{-1}	NR
20	2.61×10^{-4}	3.24×10^{-1}	NR	3.31×10^{-2}	9.87×10^{-1}	Rf

pressure (Table I), the results demonstrate that the equilibrium T_m may have been strongly dependent on the solving method for the SLE equation, although this was not the case for SRK–LCVM because we observed that calculations with this model were not sensitive to the solving method. We also observed that Rf always converged, regardless of the thermodynamic model or the system, whereas the NR method failed to converge for some systems when the SRK–WS EOS was used. On the other hand, we observed that when it converged, NR always presented similar or better results than Rf. For associated systems at atmospheric pressure (Table II), we observed that the results were independent of the method used to solve eq. (1), whereas for high-pressure SLE calculations (Table III), NR was the best method. Therefore, on the basis of these results, which cover the whole set of systems, models, and conditions, our recommendation is to use the NR method, and if it fails to converge, the Rf must be used. This recommendation was applied to the results shown in the latter sections of this article.

For all systems (except for systems 47–51 in Table IV, which were used to test the correlations), the binary interaction parameters were considered tuning parameters for the selected models through the minimization of the following objective function (OF) with the Nelder–Mead simplex method:[35]

$$\mathrm{OF} = \sum_{j=1}^{N} (T_j^{\mathrm{exp}} - T_j^{\mathrm{cal}})^2 \tag{16}$$

where superscripts "exp" and "cal" identify the experimental and calculated equilibrium temperatures, respectively. The summation was extended to the number of experimental data (N).

RESULTS AND DISCUSSION FOR SLE AT ATMOSPHERIC PRESSURE

As highlighted by Pan and Radoz,[10] the second term on the right-hand side of eq. (1) vanishes for low-pressure systems. To illustrate this, we evaluated the two terms of the right hand of eq. (1),

TABLE VII
Parameter Correlation with the Temperature for the Nonassociated Systems in SLE at Atmospheric Pressure

System	D_1	E_1	F_1	CC
SRK–LCVM (λ)				
1	-4.0000×10^{-4}	2.7940×10^{-1}	-4.8196×10^{1}	0.8927
8	1.2300×10^{-2}	-8.8830	1.6080×10^{3}	0.9909
11	-1.8700×10^{-2}	1.3529×10^{4}	-2.4405×10^{3}	0.9096
SRK–WS (WS_{12})				
1	—	—	—	—
8	-1.2700×10^{-2}	9.2445	-1.6786×10^{3}	0.9874
11	-8.5000×10^{-3}	6.5342	-1.2585×10^{3}	0.9968
PC-SAFT (K_{12})				
1	0	1.1600×10^{-3}	-4.0891×10^{-1}	0.9000
8	-1.0000×10^{-4}	1.0300×10^{-1}	-1.8486×10^{1}	0.9200
11	0	5.3000×10^{-4}	-2.2300×10^{-1}	0.9300

TABLE VIII
Average and Maximum Percentile Temperature Errors and Average Parameters for SLE at High Pressure

	PC-SAFT			SRK+LCVM			
System	K_{ij}	AAD (%)	AMD (%)	λ	UQ_{ij}	AAD (%)	AMD (%)
21	3.25×10^{-2}	0.103	0.264	0.169	0.999	1.492	3.100
22	3.34×10^{-2}	0.200	0.445	0.177	0.809	1.213	2.350
23	2.36×10^{-2}	0.047	0.096	0.346	0.319	0.591	0.850
24	2.13×10^{-2}	0.075	0.151	0.344	0.563	0.443	0.687
25	6.14×10^{-2}	0.160	0.321	0.052	0.929	0.700	1.110
26	1.10×10^{-2}	0.700	1.277	0.355	1.030	2.476	4.630
27	1.27×10^{-2}	0.761	1.367	0.226	0.658	3.704	7.210
28	1.31×10^{-2}	0.598	1.198	0.255	0.906	2.494	5.980
29	1.50×10^{-2}	0.527	1.125	0.272	0.655	2.148	4.310
30	3.96×10^{-2}	0.118	0.175	−0.122	0.785	0.880	1.280
31	4.11×10^{-2}	0.205	0.304	−0.059	1.163	0.864	1.270
32	4.29×10^{-2}	0.274	0.460	−0.080	0.950	1.080	1.680
33	4.55×10^{-2}	0.240	0.369	−0.134	1.137	1.040	1.600
34	1.21×10^{-2}	0.745	0.998	0.352	1.037	3.643	5.680
35	9.32×10^{-3}	0.472	0.914	0.345	0.667	2.083	4.870
36	8.92×10^{-3}	0.554	0.932	0.403	0.357	1.876	3.330
37	3.45×10^{-2}	0.077	0.116	0.025	0.414	0.235	0.356
38	3.94×10^{-2}	0.114	0.200	−0.006	1.539	0.366	0.626
39	4.31×10^{-2}	0.453	0.714	0.106	0.832	1.572	3.080
40	4.58×10^{-2}	0.525	0.833	0.063	0.831	2.148	3.600
41	4.87×10^{-2}	0.445	0.920	0.048	0.997	1.833	3.290
42	3.57×10^{-2}	0.536	1.473	0.171	0.844	1.599	3.870
43	4.50×10^{-2}	0.065	0.097	−0.031	1.143	0.268	0.400
44	1.66×10^{-2}	0.476	1.167	−0.149	1.358	1.554	3.670
45	3.75×10^{-2}	0.065	0.096	0.425	2.043	0.067	0.239
46	2.67×10^{-2}	0.248	0.456	CNA	CNA	CNA	CNA

CNA = convergence not achieved.

using the PE–heptane system at 348 K and atmospheric pressure:

$$\frac{\Delta H_u}{RT_m} \times \left(\frac{T_m}{T} - 1\right) = 474.46$$

$$\frac{\Delta vP}{RT} = 1.7288 \times 10^{-4}$$

Therefore, we carried out atmospheric pressure calculations, neglecting the second term on the right-hand side of eq. (1).

Parameter estimation for nonassociated systems

For each system, the parameters were fitted for each experimental datum, and an average parameter value for each system was obtained by the division of its sum by the number of experimental data. These average parameter values were applied once more to the calculation and the prediction of the temperature. Table V shows the percentage absolute average deviation (AAD) and the percentage absolute maximum deviation (AMD) calculated for the first 11 nonassociated systems at atmospheric pressure, as described in Table I. The table also shows the method used to solve eq. (1) according to the recommendation described earlier. For these nonassociated systems evaluated at atmospheric pressure, the results indicate SRK–LCVM as the most accurate model. It may be rather surprising that SRK–LCVM showed better behavior than PC-SAFT, as the latter has been widely and successfully applied to polymer systems. It seems that at low pressure, the complexity of PC-SAFT, which is more adequate for describing polymer systems, was less important than the number of adjusted parameters. Therefore, the models with more adjusted parameters (two in the SRK models) presented smaller errors than

TABLE IX
PC-SAFT Parameter Correlation at High Pressure

System	G_1	H_1	I_1	J_1
PE–propane	5.0070×10^{-1}	-8.9686×10^{1}	1.1680×10^{-7}	3.5030×10^{-3}
PE–ethane	-5.9346×10^{1}	-3.3825×10^{2}	3.2729×10^{-8}	-1.6157×10^{-2}

TABLE X
SRK–LCVM Parameter Correlation at High Pressure

	System	
Parameter	PE–propane	PE–ethane
A_2	1.0574×10^{3}	1.9132
B_2	-2.7166×10^{2}	-4.1530×10^{-5}
C_2	1.7504×10^{1}	1.0276×10^{-1}
D_2	-2.2670×10^{-6}	-8.8248×10^{3}
E_2	-3.6472×10^{-1}	1.8130×10^{-5}
F_2	-2.2398×10^{-1}	-2.6840×10^{-2}
G_2	1.8620×10^{-7}	1.8930×10^{15}
H_2	1.6290×10^{-1}	0

PC-SAFT, where only one parameter was fitted. Moreover, the sophisticated mixing rules of SRK are based on models that are very suitable for describing the low-pressure equilibrium of complex systems.

An interesting result shown in Table V is system 11 because, in this case, the solvent (paraffin wax) was a mixture of unknown composition. Only its chemical structure and MW were available, and SLE calculations were carried out with only this information; notwithstanding, good results were obtained, regardless of the model.

Parameter estimation for the associated systems

Table VI shows the average and maximum percentage temperature errors obtained for the associated systems at atmospheric pressure, with the same averaging procedure adopted over the estimated parameters described earlier. All of the calculations were carried out with only the SRK equation because of the best performance achieved with the nonassociated systems at atmospheric pressure. The results show that the calculated data were in excellent agreement with the experimental data for all selected systems, mainly when the complex chemical nature of the solvents was highlighted.

TABLE XI
Average Percentile Temperature Error Obtained with the Correlated Parameters for SLE at High Pressure

	PC-SAFT			SRK–LCVM			
System	$(K_{ij})^{ad}$	AAD (%)	AMD (%)	λ^{ad}	$(UQ_{ij})^{ad}$	AAD (%)	AMD (%)
21	3.32×10^{-2}	0.137	0.401	1.700×10^{-1}	9.150×10^{-1}	1.486	3.070
22	3.26×10^{-2}	0.258	0.412	1.758×10^{-1}	9.101×10^{-1}	1.155	2.390
23	2.27×10^{-2}	0.199	0.294	3.438×10^{-1}	4.338×10^{-1}	0.518	0.927
24	2.21×10^{-2}	0.154	0.245	3.467×10^{-1}	4.290×10^{-1}	0.530	0.759
25	6.14×10^{-2}	0.159	0.322	5.200×10^{-2}	9.376×10^{-1}	0.699	1.110
26	2.48×10^{-2}	3.299	4.632	2.340×10^{-1}	9.108×10^{-1}	3.628	6.940
27	2.47×10^{-2}	2.840	4.260	2.795×10^{-1}	9.283×10^{-1}	3.256	5.640
28	2.42×10^{-2}	2.445	3.682	2.203×10^{-1}	8.814×10^{-1}	2.875	6.330
29	2.30×10^{-2}	1.509	2.653	3.948×10^{-1}	5.681×10^{-1}	2.801	5.360
30	2.59×10^{-2}	2.944	3.099	1.125×10^{-2}	6.597×10^{-1}	2.713	4.070
31	2.57×10^{-2}	3.280	3.559	2.191×10^{-1}	9.194×10^{-1}	5.631	7.210
32	2.52×10^{-2}	3.602	3.937	2.974×10^{-1}	9.332×10^{-1}	7.307	9.420
33	2.45×10^{-2}	3.989	4.287	6.038×10^{-2}	8.203×10^{-1}	3.756	5.290
34	1.40×10^{-2}	0.752	1.452	1.963×10^{-1}	9.326×10^{-1}	4.818	8.250
35	1.20×10^{-2}	0.607	1.524	2.082×10^{-1}	9.112×10^{-1}	5.074	7.550
36	7.86×10^{-3}	0.577	0.948	2.662×10^{-1}	5.981×10^{-1}	2.955	5.530
37	4.14×10^{-2}	1.493	1.606	-8.683×10^{-2}	4.773×10^{-1}	2.502	2.810
38	4.16×10^{-2}	0.449	0.637	2.119×10^{-1}	9.785×10^{-1}	4.590	5.380
39	4.03×10^{-2}	0.628	1.037	1.320×10^{-1}	9.713×10^{-1}	1.741	2.970
40	4.06×10^{-2}	1.019	1.593	1.236×10^{-1}	9.349×10^{-1}	2.329	4.530
41	4.10×10^{-2}	1.315	1.770	2.019×10^{-1}	6.200×10^{-1}	3.061	5.740
42	4.01×10^{-2}	0.980	2.469	1.155×10^{-1}	9.816×10^{-1}	1.838	5.030
43	4.13×10^{-2}	0.716	0.770	-4.027×10^{-2}	1.014	0.332	0.487
44	—[a]	—[a]	—[a]	—[a]	—[a]	—[a]	—[a]
45	—[a]	—[a]	—[a]	—[a]	—[a]	—[a]	—[a]
46	—[a]	—[a]	—[a]	—[a]	—[a]	—[a]	—[a]
47	1.41×10^{-2}	1.789	2.573	1.88×10^{-1}	9.29×10^{-1}	7.267	9.730
48	4.14×10^{-2}	0.389	0.458	5.17×10^{-2}	8.92×10^{-1}	0.476	0.719
49	4.03×10^{-2}	0.809	1.202	1.24×10^{-1}	9.68×10^{-1}	2.170	3.640
50	4.13×10^{-2}	0.177	0.200	-2.29×10^{-1}	8.20×10^{-1}	6.596	8.120
51	4.13×10^{-2}	0.375	0.574	5.41×10^{-2}	1.09	8.981	9.500

[a] The experimental polymer concentration was insufficient to obtain a parameter correlation.

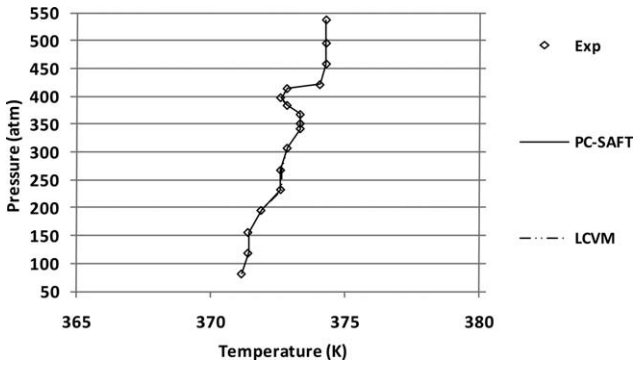

Figure 1 Solid–fluid phase transitions of the PE–pentane system: MW = 121,000 and WT = 5 (system 44).

Predictive correlations

SLE calculations can be very useful to predict equilibrium T_m values for compositions where experimental data are not available. Therefore, for systems 1, 8, and 11, which presented the largest numbers of experimental data, parameter correlations as a function of temperature were obtained with standard least-squares procedures applied to the optimal interaction parameter found earlier. The parameter functional forms are presented in eqs. (17)–(19), and their coefficients and correlation coefficients (CCs) for each model are shown in Table VII (the UNIQUAC UQ_{12} parameters, in general, did not correlate well with the temperature):

$$\lambda = D_1T^2 + E_1T + F_1 \quad (17)$$

$$WS_{12} = D_1T^2 + E_1T + F_1 \quad (18)$$

$$K_{12} = D_1T^2 + E_1T + F_1 \quad (19)$$

where D_1, E_1, and F_1 are constants. For the SRK–LCVM model, parameter correlations (λ's) were quadratically dependent on the temperature and gave good results. The same observations were made for the SRK–WS model (WS_{12} parameter) with systems 8 and 11, whereas for system 1, it was not possible to obtain a good parameter correlation because of the poor results obtained, as shown in Table V. The results for the PC-SAFT model show good simple correlations for the adjusted K_{12} parameter. For nonassociated systems, insufficient experimental data were available to develop good correlations.

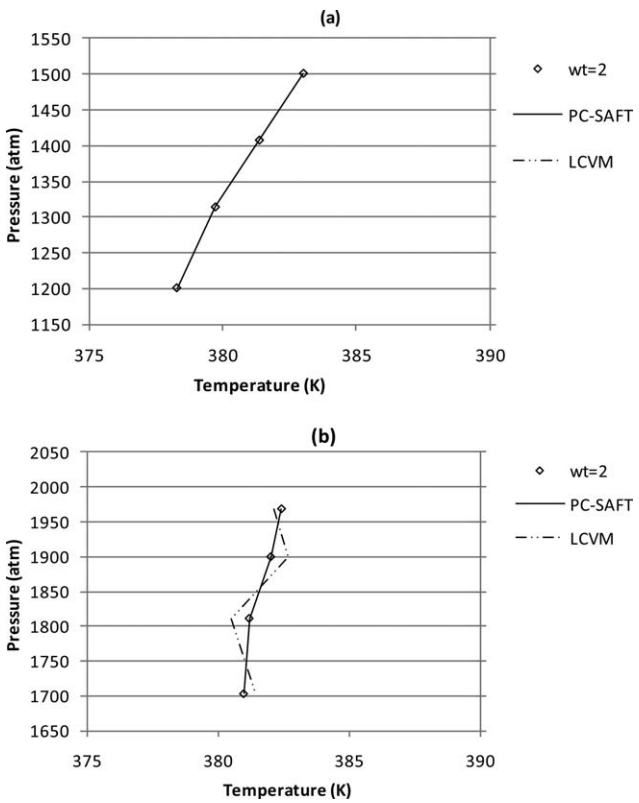

Figure 2 Solid–fluid phase transitions of the PE–ethylene system: (a) MW = 7000 and WT = 2 (system 45) and (b) MW = 23,625 and WT = 2 (system 46).

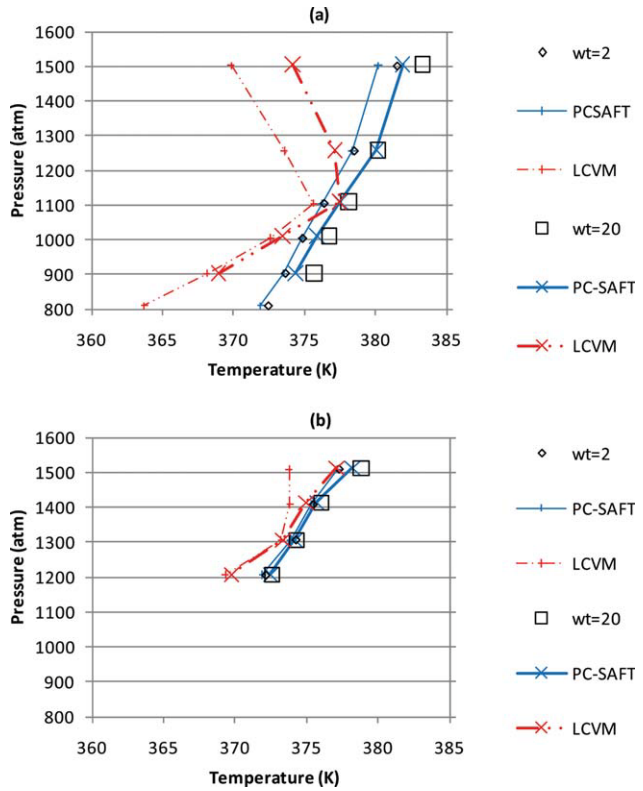

Figure 3 Solid–fluid phase transitions of the PE–ethane system: (a) MW = 7000 and WT = 2 and 20 (systems 21 and 22, respectively) and (b) MW = 23,625 and WT = 2 and 20 (systems 23 and 24, respectively). [Color figure can be viewed in the online issue, which is available at wileyonlinelibrary.com.]

RESULTS AND DISCUSSION FOR SLE AT HIGH PRESSURE

Parameter estimation

The three models, PC-SAFT, SRK–WS, and SRK–LCVM, were applied to the systems and are

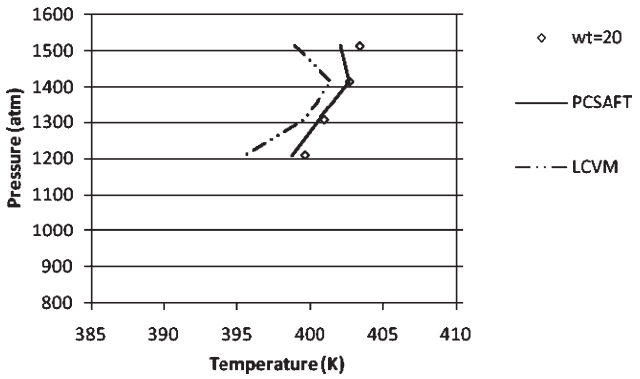

Figure 4 Solid–fluid phase transitions of the PE–ethane system: MW = 52,000 and WT = 20 (system 25).

presented in Table III for high-pressure SLE calculation. The same parameter averaging procedure described previously was used, but for SRK–WS, the parameter range for each evaluated system was too large and, therefore, did not allow the use of average parameter values. This was unexpected because the WS mixing rule was originally developed to extend the cubic EOS for high-pressure applications. Few differences were observed among the parameter values at moderate pressures, but at the high-pressure level, it was impossible to achieve good results, regardless of the estimated initial parameters; therefore, we did not take the SRK–WS results further (see the Appendix for these results).

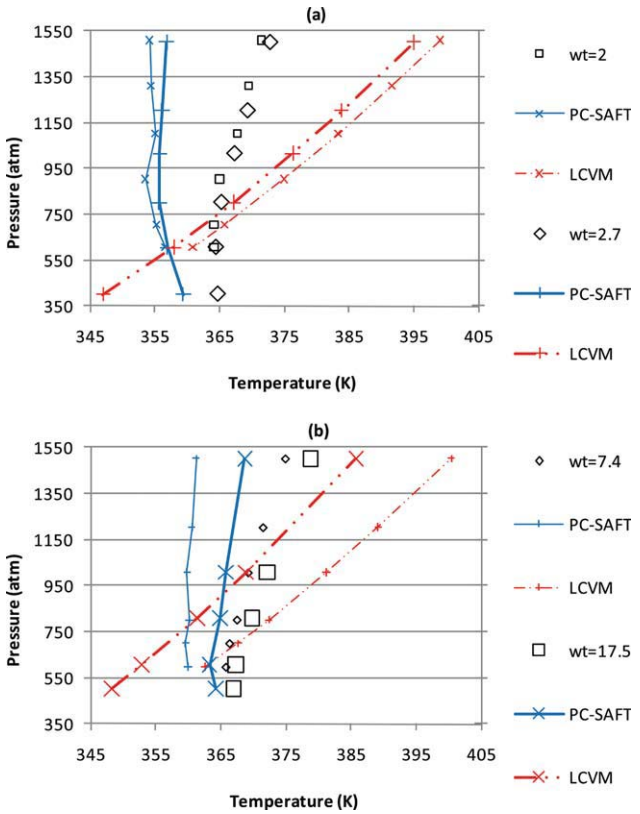

Figure 5 Solid–fluid phase transitions of the PE–propane system: (a) MW = 7000 and WT = 2 and 2.7 (systems 26 and 27, respectively) and (b) MW = 7000 and WT = 7.4 and 17.5 (systems 28 and 29, respectively). [Color figure can be viewed in the online issue, which is available at wileyonlinelibrary.com.]

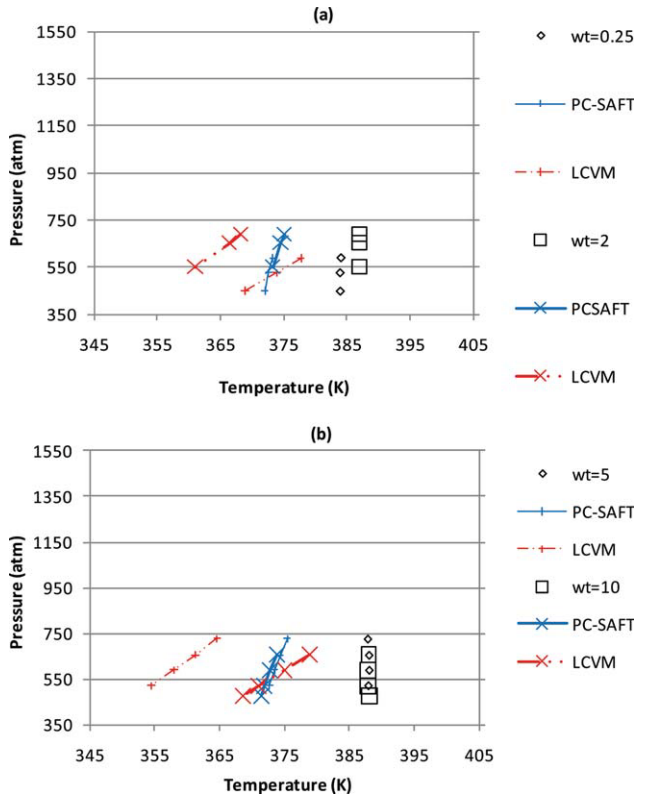

Figure 6 Solid–fluid phase transitions of the PE–propane system: (a) MW = 13,600 and WT = 0.25 and 2 (systems 30 and 31, respectively) and (b) MW = 13,600 and WT = 5 and 10 (systems 32 and 33, respectively). [Color figure can be viewed in the online issue, which is available at wileyonlinelibrary.com.]

Table VIII summarizes the analyses of the results from the PC-SAFT and SRK–LCVM EOSs. Although average parameters were used, the corresponding AAD was extremely low. The calculated results presented in Table VIII show that LCVM gave good results when the G^E mixing rule model and the equation solving method were efficient, although this mixing rule was not originally developed for high-pressure SLE. Another aspect worth highlighting is that only one parameter was sufficient to give good results with the PC-SAFT EOS.

Predictive correlations

From a practical viewpoint, it is important for an EOS to be robust with regard to extrapolation, as is shown in the section on Interpolating and Extrapolating Parameter Correlations for the Systems Not Used in the Parameter Estimation. Nevertheless, even if one does not intend to extrapolate the application of

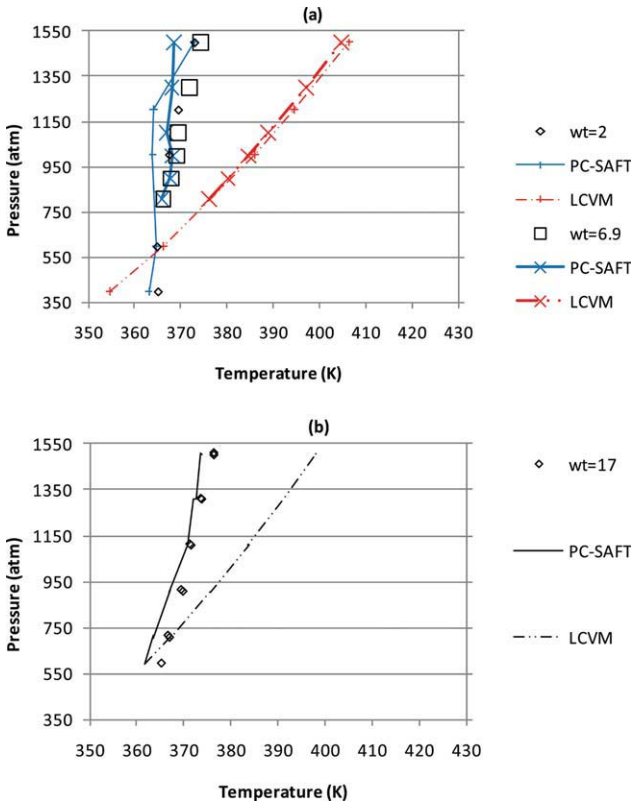

Figure 7 Solid–fluid phase transitions of the PE–propane system: (a) v = 23,625 and WT = 2 and 6.9 (systems 34 and 35, respectively) and (b) MW = 23,625 and WT = 17 (system 36). [Color figure can be viewed in the online issue, which is available at wileyonlinelibrary.com.]

the model or doubt its predictive capabilities, parameter correlations are a very suitable method for modeling interpolations. Therefore, we looked for predictive parameter correlations for the PC-SAFT and SRK–LCVM models.

The fitted parameters were put into groups according to the selected polymer–solvent systems (PE–ethane and PE–propane), and all of the respective experimental data presented in Table III were used. Then, a correlation was generated with MW and percentage weight polymer concentration (WT) as independent variables. Equation (20) shows the PC-SAFT parameter correlation for the PE–propane (96 experimental data points) and PE–ethane (23 experimental data points) systems. The numerical values of the constants are shown in Table IX:

$$K_{ij}(\mathrm{MW},\mathrm{WT}) = \frac{G_1 + \frac{\mathrm{WT}}{100.0}}{H_1 + I_1 \times \mathrm{MW}^2} + J_1[\ln \mathrm{MW}] \quad (20)$$

where G_1, H_1, I_1, and J_1 are constants. It is important to note the large MW range considered in this adjustment. As a result of these parameter correlations, the calculation became a completely predictive task because the only properties that had to be known were MW and WT. When data from other alkane solvents were available, we could even try a correlation with the number of carbons or a group contribution approach.

The same experimental data were used to obtain correlations for the LCVM parameters λ and UQ_{ij}. The resulting expressions are shown in eqs. (21) and (22), and their corresponding coefficients are shown in Table X:

$$\lambda(\mathrm{MW},\mathrm{WT}) = A_2\left(\frac{\mathrm{WT}}{100.0}\right)^3 + B_2\left(\frac{\mathrm{WT}}{100.0}\right) + C_2\left(\frac{\mathrm{WT}}{100.0}\right) + D_2\mathrm{MW} \quad (21)$$

$$\mathrm{UQ}_{ij}(\mathrm{MW},\mathrm{WT}) = \frac{E_2 + \left(\frac{\mathrm{WT}}{100}\right)}{F_2 + G_2\mathrm{MW}} + H_2 \times \ln\left(\frac{\mathrm{WT}}{100}\right) \quad (22)$$

where A_2, B_2, C_2, D_2, E_2, F_2, G_2, and H_2 are constants. Table XI presents the adjusted model parameters and average and maximum percentage temperature errors for SLE. The developed correlations obtained from a wide data set were applied to each system, and the average percentage temperature error was calculated. With this calculation, we could analyze

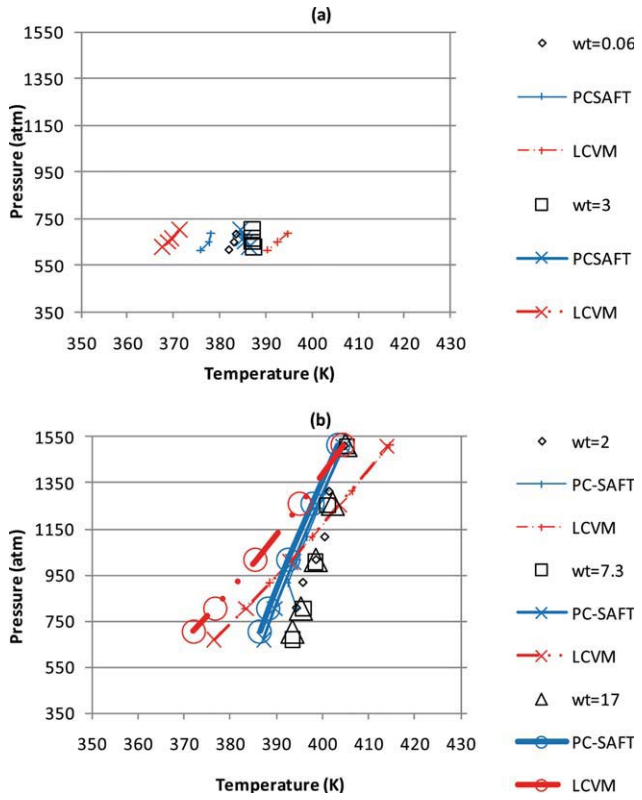

Figure 8 Solid–fluid phase transitions of the PE–propane system: (a) MW = 42,900 and WT = 0.06 and 3 (systems 37 and 38, respectively) and (b) MW = 52,000 and WT = 2, 7.3, and 17 (systems 39, 40, and 41, respectively). [Color figure can be viewed in the online issue, which is available at wileyonlinelibrary.com.]

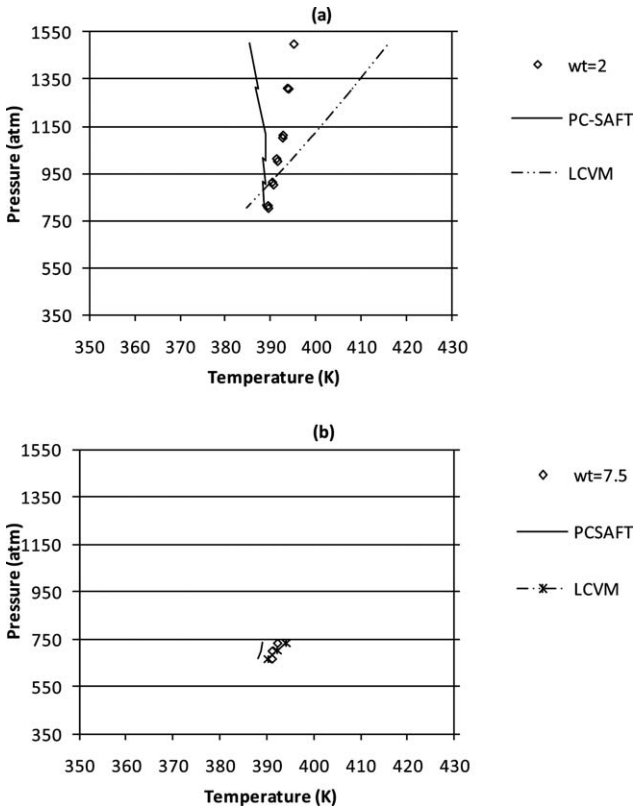

Figure 9 Solid–fluid phase transitions of the PE–propane system: (a) MW = 59,300 and WT = 2 (system 42) and (b) MW = 119,600 and WT = 7.5 (system 43).

the behavior in each of the systems investigated and, to some extent, evaluate the fitting quality. The results demonstrate good performance of the PC-SAFT equation, and it was worthwhile to highlight the performance in describing systems 47–51, which were not used in the fitting procedure. With regard to systems 44–46 (pentane and ethylene systems), there were no results because various data of polymer concentration and/or MW were not at our disposal, so a correlation could not be developed.

We performed a detailed assay by analyzing the AAD percentage values for each system. For systems 26–43 (PE–propane systems used on correlation development), with the PC-SAFT equation, the maximum AAD percentage with fitted parameters was 3.989 for system 33, and the AMD percentage was 4.632 for system 26. Even systems with a high polymer concentration and large pressure and temperature ranges, such as systems 41 and 42, exhibited ADD percentages equal to 1.315 and 0.980 and AMD percentages equal to 1.770 and 2.469, respectively. Comparing the SRK–LCVM and PC-SAFT models, we observed that SRK–LCVM EOS gave a larger AAD percentage, and its maximum value was 7.307; this was achieved with system 32, which also showed an AMD percentage equal to 9.420. Because this model was not originally developed for SLE calculation, these errors could be considered small. For the PE–ethane systems (21–25), the PC-SAFT EOS once again showed better results than the SRK–LCVM EOS; the highest AAD percentage was 0.258 for system 22, which also showed an AMD percentage equal to 0.412, although the performance of the SRK–LCVM EOS was quite good, with a maximum AAD percentage equal to 1.486 and a AMD percentage equal to 3.070 (both for system 21).

Graphic analysis of the solvent, pressure range, polymer MW, and composition effects on the model performance

Calculations with the average estimated parameters

To further evaluate the average parameters estimated in the Parameter Estimation section, some of these parameters were applied to the corresponding system to observe the influence of the solvent, pressure range, and polymer MW on the performance of the models. The PE–pentane and PE–ethylene systems were selected for these calculations as only one MW and one polymer concentration data point were available for the first system and only one polymer concentration data point was available for

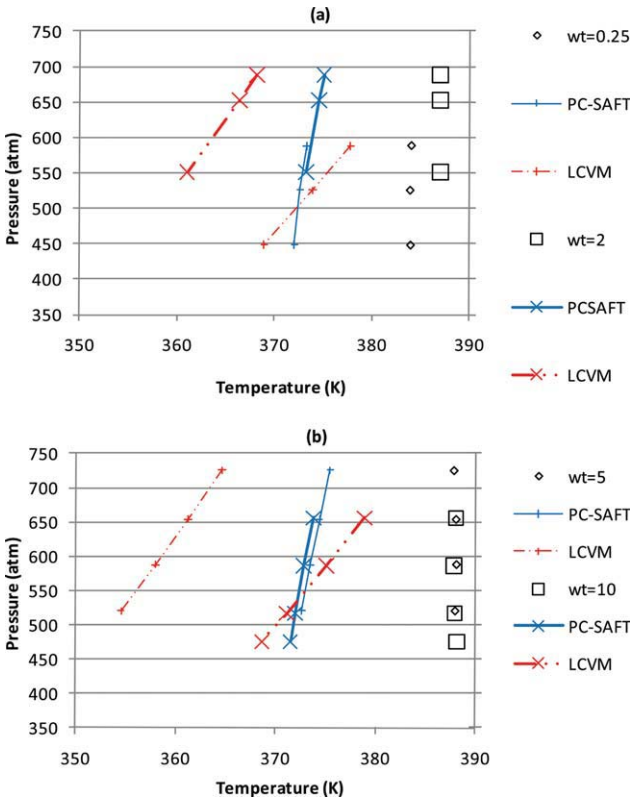

Figure 10 Solid–fluid phase transitions of the PE–propane system: (a) magnification of Figure 6(a) and (b) magnification of Figure 6(b). [Color figure can be viewed in the online issue, which is available at wileyonlinelibrary.com.]

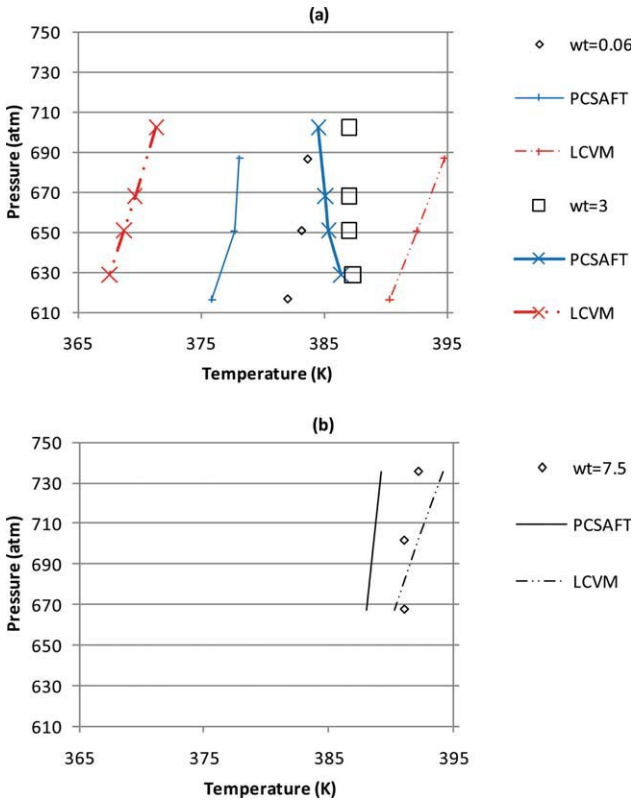

Figure 11 Solid–fluid phase transitions of the PE–propane system: (a) magnification of Figure 8(a) and (b) magnification of Figure 9(b). [Color figure can be viewed in the online issue, which is available at wileyonlinelibrary.com.]

the second system. It was, therefore, not possible to develop a parameter correlation, as stated earlier and as shown in Table III.

Figure 1 shows the solid–fluid phase transition calculations for the PE–pentane system. The results indicate that there was no difference between the experimental data and those of the PC-SAFT equation and the LCVM–SRK model. The ethylene system results are shown in Figure 2. Figure 2(a) shows similar performances for the two models. Figure 2(b) shows the excellent performance of the PC-SAFT model and the good performance of the cubic LCVM–SRK EOS.

Calculations with the predictive correlations

To further evaluate the fitting procedures developed in the Predictive Correlations section, the developed parameter correlations were applied to the ethane and propane systems. To show the influence of the selected model, the polymer MW, and the polymer weight fraction, Figures 3 and 4 (ethane systems) and Figures 5–9 (propane systems) show the solid–fluid phase transitions of the analyzed systems. Figures 10 and 11 show magnifications of some of the graphs in Figures 5–9 to emphasize their details.

Figure 3(a) shows the behavior of both models with a low polymer MW. The simulation results indicate excellent performance with the PC-SAFT model with parameters from the developed correlation. With LCVM–SRK, although we observed a reasonable performance at the lower bound of the considered pressure range, the overall behavior was poor because this model failed in the qualitative description of the phenomenon. The same general observations applied to Figures 3(b) and 4, and therefore, we observed that for this PE–ethane system, the model performances were insensitive with regard to the polymer MW.

Figure 5(a) shows the excellent behavior of the PC-SAFT equation in describing this PE–propane system. Despite the small difference between the weight fractions of the two data sets, the model captured this difference for the whole high-pressure range. The performance of the LCVM was not good, with a systematic slope mismatch that was also observed throughout virtually all of the other simulations, shown in Figures 5–9. Figure 5(b), with the same polymer MW and higher concentrations shown in Figure 5(a), also shows good simulation results with the PC-SAFT equation for both polymer concentrations. With SRK–LCVM, the error between the

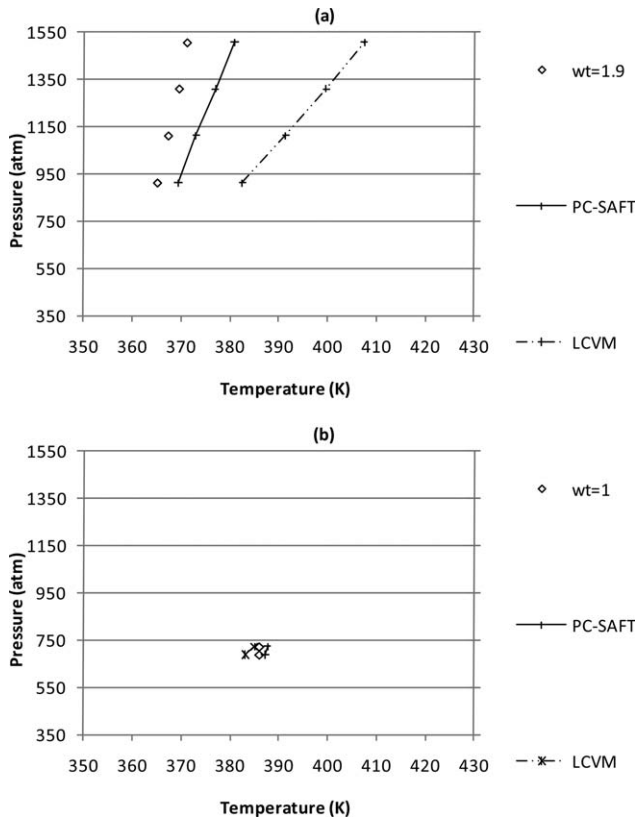

Figure 12 Solid–fluid phase transitions of the PE–propane systems not used in the parameter estimation: (a) MW = 23,625 and WT = 1.9 (system 47) and (b) MW = 42,900 and WT = 1 (system 48).

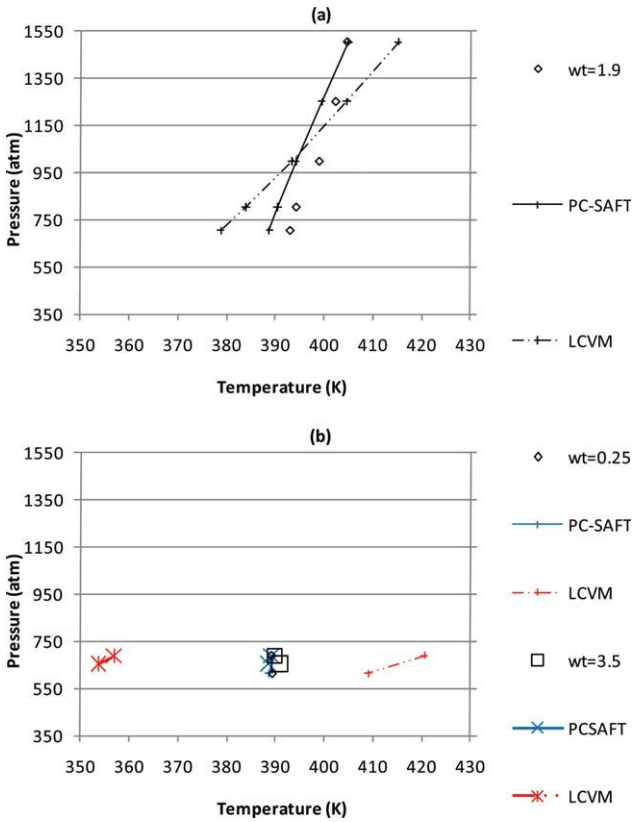

Figure 13 Solid–fluid phase transitions of the PE–propane systems not used in the parameter estimation: (a) MW = 52,000 and WT = 1.9 (system 49) and (b) MW = 119,600 and WT = 0.25 and 3.5 (systems 50 and 51, respectively). [Color figure can be viewed in the online issue, which is available at wileyonlinelibrary.com.]

experimental data and the simulation results at the highest concentration increased as the pressure decreased and the opposite behavior was observed at the lowest polymer concentration. As shown Figures 6(a) and 10(a) (the magnification), with a higher polymer MW, the PC-SAFT equation was not able to precisely distinguish the difference between the polymer weight fractions. This model's low sensitivity with regard to weight fraction is also shown in Figure 6(b) [with the same polymer MW and higher concentrations than those shown in Figs. 6(a) and 10(b) (the magnification) but, in this case, in accordance with experimental data]. As the polymer MW increased, as shown in Figure 7(a,b), we observed excellent results with the PC-SAFT simulations. With the LCVM–SRK model, there was an increase in the simulation error as the pressure increased. This same trend was observed with other polymer MWs and other polymer concentrations.

Whereas Figures 5–7 show low- and medium-MW polymer data, Figures 8 and 9 show the results for higher MW systems. Figures 8(a) and 11(a) (the magnification) show excellent results for the PC-SAFT model, especially for the 3% polymer weight fraction. There were different trends with regard to the LCVM–SRK model: an overestimation with the smallest polymer weight fraction and an underestimation with the highest one. Figure 8(b) shows the excellent performance of the PC-SAFT model for all three polymer concentrations. As shown in Figure 9(a), there was an increasing difference between the experimental and simulated temperatures with increasing pressure for both correlation models. A remarkable model mismatch was observed with the LCVM–SRK equation, shown in Figure 9(a), although, as shown in Figures 9(b) and 11(b) (the magnification), with the highest investigated MW, we observed excellent behavior with this model.

In summary, Figures 5–11 show that PC-SAFT had a very good overall performance, clearly superior to that of LCVM–SRK. Moreover, the PC-SAFT model performed better at higher polymer concentrations,

TABLE XII
PE–Propane Temperature Calculation with the Correlated Parameters

System	MW	Polymer concentration	T^{exp} (K)	T^{calc} (PC-SAFT)	T^{calc} (SRK–LCVM)	Pressure (atm)
47	23,625	1.9	365.307	369.428	382.576	911.628
			367.535	373.081	391.447	1110.594
			369.763	376.970	399.756	1309.561
			371.377	380.931	407.497	1504.910
48	42,900	1	385.954	387.723	385.054	721.723
			385.961	387.199	383.185	688.462
49	52,000	1.9	404.734	404.988	415.196	1503.423
			402.375	399.495	404.676	1250.667
			399.024	394.226	393.359	997.963
			394.308	390.482	383.912	803.969
			393.067	388.754	378.755	705.081
50	119,600	0.25	389.020	389.799	420.614	690.245
			389.230	388.625	408.971	613.038
51	119,600	3.5	389.858	389.166	356.873	687.050
			390.858	388.614	353.717	652.734

regardless of the polymer chain length. A slightly better performance of the PC-SAFT model in describing ethane systems (Figs. 3 and 4) than in describing propane systems (Figs. 5–11) was also observed.

Interpolating and extrapolating parameter correlations for the systems not used in the parameter estimation

Figures 12 and 13 present results with systems not used in the fitting procedure, and Table XII details these results and shows the calculated and experimental values. With these results, it was, therefore, possible to evaluate the fitting performance. The results of systems 47–48 and 50–51 represent weight polymer concentration extrapolations with regard to the parameter correlations developed, whereas the results of system 49 represent an interpolation calculation. The simulation results show the excellent behavior of the PC-SAFT equation. The same evaluation could not be carried out with the SRK–LCVM model, except for the simulation of the 42,900 polymer MW system, where the results were considered excellent. A number of factors must have influenced these results. For example, with the lowest MW, a higher pressure level was observed, and given this, the mixing rule was unable to cope with the equilibrium description. Even with the PC-SAFT equation, there was an increased simulation error with increasing pressure for this system. When the results with the 52,000 polymer MW system were analyzed, no systematic behavior with regard to pressure variations was observed. On the other hand, despite the low pressure level with the 119,600 polymer MW system, the SRK–LCVM simulation errors were considered relevant.

CONCLUSIONS

SLEs for PE and PP solutions with different solvents were modeled with the SRK cubic EOS (with LCVM and WS mixing rules) and PC-SAFT EOS. The focus of this study was to compare the performances of these models in describing SLE phase behavior. This new approach is different from those usually found in the literature, in which the effects of crystallinity and MW on SLE were investigated.

Regardless of the model used to simulate SLE, a key variable in the analysis of the results is the pressure level. As pointed out by Pan and Radoz,[10] the second term on the right-hand side of eq. (1) vanishes for low-pressure systems. So with these simulations, the pressure effect is restricted to the ϕ_p^L and ϕ_p^0, which are related to the selected EOS. On the other hand, high-pressure conditions are quite difficult to model because the pressure influences both sides of the SLE equation.

The PC-SAFT and SRK EOSs, with two different mixing rules (LCVM and WS), were used and compared. An experimental database at atmospheric pressure containing 20 polymer–solvent systems was considered. The influence of the method used for solving the SLE equation to obtain T_m was also investigated. The calculated results indicate SRK–LCVM as the best model at atmospheric pressure conditions. However, it is important to highlight that with the SRK–LCVM model, two adjusted parameters were used in the simulation: one related to the mixing rule and another related to the G^E model selected. When the predictive ability of the SRK–LCVM model was evaluated, we observed that it was not easy to generate a good correlation of the G^E parameter (WT_{12}) with the temperature. This difficulty was not observed with the PC-SAFT EOS because the only fitted parameter correlated very well with the temperature for all of the systems analyzed.

Another database containing 31 polymer–solvent systems at high pressure was used, and under these conditions, the sensitivity of the EOS with regard to pressure was noticeable as the pressure influence on the right-hand side of the SLE equation had to be taken into consideration. Surprisingly, the SRK–WS model was not appropriate for high-pressure SLE calculation in these systems. Interaction parameter correlations as a function of MW and polymer concentration were developed for the PC-SAFT and SRK–LCVM EOSs. The PC-SAFT EOS with parameter correlation provided the best performance. The results were excellent for the PC-SAFT equation with various hydrocarbon solvents, especially for higher polymer concentrations, regardless of the polymer chain length or the pressure range. The predictive abilities of the PC-SAFT and SRK–LCVM EOSs were evaluated by the testing of five systems not used in the fitting procedure. Once more, PC-SAFT and the developed parameter correlation presented good results and showed suitable interpolating and extrapolating features.

NOMENCLATURE

a	parameter of the SRK EOS
A	Helmholtz free energy per number of molecules
A_2, B_2, C_2, and D_2	constants [eq. (21)]
A_i, B_i, and C_i	group volume temperature constants in the GCVOL method
A_M and A_v	parameters of the LCVM mixing rule
AAD	percentage absolute average deviation
AMD	percentage absolute maximum deviation
b	parameter of the SRK EOS

BV	Bogdanic and Vidal
c	crystallinity fraction
CC	correlation coefficient
d	numerical constant of the WS mixing rule [eq. (6)]
D_1, E_1, and F_1	constants [eqs. (17)–(19)]
E_2, F_2, G_2, and H_2	constants [eq. (22)]
entr-FV	entropic free volume
EOS	equation of state
FV	free volume
G_1, H_1, I_1, and J_1	constants [eq. (20)]
GCVOL	group contribution volume
G^E	Gibbs free energy
ΔH_u	enthalpy of melting per moles of crystal units
k	Boltzmann constant
K_{ij}	adjustable binary interaction parameter of the PC-SAFT EOS [eq. (4)]
LCVM	linear combination of the Vidal and Michelsen mixing rules
MW	molecular weight
N	total number of molecules or number of experimental data
n_i	number of group i in the GCVOL method
ncomp	number of components
NR	Newton–Raphson
nseg	number of segments
OF	objective function
P	pressure
PC-SAFT	perturbed-chain statistical associating fluid theory
PE	polyethylene
PP	polypropylene
R	gas constant
Rf	Regula–falsi
SLE	solid–liquid equilibrium
SRK	Soave–Redlich–Kwong
T	temperature
T_m	melting temperature
u	number of monomer units in the polymer backbone
UNIQUAC	Universal quasi-chemical
UQ_{ij}	interaction parameter of the LCVM mixing rule [eq. (22)]
v	molar volume
Δv	polymer volume change
$V_{W,i}$	van der Waals volume
WS	Wong–Sandler
WS_{ij}	binary interaction parameter of the WS mixing rule [eq. (8)]
WT	percentage weight polymer concentration
x	molar fraction (solubility)
X	molar fraction of the segment

Greek letters

α and λ	parameters of the LCVM mixing rule [eq. (9)]
β	FV fraction
δ	number of segments in the component
ε	dispersion energy parameter
γ	molar activity coefficient
ϕ	fugacity coefficient
ρ_a	density of an amorphous polymer
ρ_c	density of a crystalline polymer
σ	segment diameter

Superscripts

0	pure liquid polymer
ad	adjusted
assoc	association contribution
cal	calculated
disp	dispersion contribution
exp	experimental
hc	hard chain contribution
L	polymer in solution
res	residual

Subscripts

i	component or group i
j	component or group j
k, m, and n	segments
p	polymer
W	van der Waals

APPENDIX

SLE calculations at high pressure with the SRK–WS model

Table XIII shows the PE–propane temperature calculations with the SRK–WS model with adjusted parameters for each set of MW/polymer concentration data, that is, without the correlation of the adjusted parameters with MW and polymer concentration. It was impossible to obtain a parameter correlation with this model because of the large scattering of fitted parameters. For this reason, the results are presented in a different fashion, only through tabulated values instead of the graphic displays presented for the previous results. The simulation results showed a systematic performance: higher deviations from the experimental data were observed with increased polymer MW.

TABLE XIII
PE–Propane Temperature Calculation with the SRK–WS Model Without Correlation of the Adjusted Parameters with MW and Polymer Concentration

MW	Polymer concentration (system)	T^{exp} (K)	T^{calc} (SRK–WS)	Pressure (atm)
7000	2 (26)	371.453	371.452	1509.604
		369.471	367.485	1310.734
		367.709	360.629	1102.824
		365.066	361.385	903.954
		364.185	364.184	705.084
		364.185	364.184	605.649
	2.7 (27)	364.691	364.689	401.219
		364.403	364.401	606.097
		365.267	365.264	802.439
		367.283	359.038	1015.853
		369.300	368.199	1203.658
		372.757	368.199	1502.439
	7.4 (28)	365.843	365.840	597.560
		366.419	366.417	700.000
		367.572	367.566	802.439
		369.300	364.260	1007.317
		371.604	364.260	1203.658
		375.061	361.038	1502.439
	17.5 (29)	366.995	366.993	503.658
		367.283	367.279	606.097
		369.876	369.874	810.975
		372.181	368.383	1007.317
		378.806	375.979	1502.439
13,600	0.25 (30)	384.074	383.483	587.995
		383.926	383.537	525.488
		383.960	382.629	448.704
	2 (31)	387.000	383.172	688.126
		387.015	382.135	652.412
		387.060	385.663	550.628
	5 (32)	387.857	379.446	725.664
		388.062	381.779	654.244
		388.091	385.752	588.174
		387.946	384.226	520.311
	10 (33)	388.062	385.054	656.030
		387.917	384.408	586.381
		387.948	384.200	516.739
		388.140	384.348	475.676
23,625	2 (34)	365.066	365.062	397.740
		364.845	364.844	596.610
		367.488	360.195	1003.389
		369.471	361.755	1202.259
		372.995	361.755	1500.564
	6.9 (35)	366.285	366.280	804.790
		368.000	367.995	897.005
		369.142	367.995	997.604
		369.428	367.435	1098.203
		372.000	367.435	1299.401
		374.285	363.385	1500.598
	17 (36)	366.857	366.854	704.191
		369.714	369.154	905.389
		371.428	369.154	1106.586
		373.714	367.957	1307.784
		376.285	367.957	1500.598
		365.116	365.113	591.751
		366.511	366.509	713.452
		369.302	367.169	912.655
		371.162	370.889	1111.756
		373.488	367.362	1310.908
		376.279	367.362	1510.111
42,900	0.06 (37)	383.666	382.358	686.780
		383.166	382.051	650.861
		382.000	381.720	616.623
	3 (38)	387.000	385.912	702.307
		387.000	383.806	668.119
		387.000	383.004	651.025
		387.333	384.225	628.817
52,000	2 (39)	404.722	385.869	1513.198
		401.481	382.067	1313.945
		400.555	368.725	1114.947
		398.703	368.725	1015.295
		395.925	381.743	915.541
		394.537	382.642	804.890
	7.3 (40)	393.606	383.860	667.103
		395.901	380.073	803.139
		398.483	380.073	1007.088
		401.065	380.073	1253.462
		405.368	380.073	1508.529
	17 (41)	405.116	385.942	1513.298
		402.325	385.591	1258.846
		398.604	385.448	1015.341
		395.348	385.562	805.036
		393.488	385.438	705.383
59,300	2 (42)	389.444	378.099	815.377
		390.370	381.555	914.927
		391.296	381.555	1014.477
		392.685	368.546	1114.078
		393.611	368.546	1313.075
		395.022	353.985	1500.564
		393.920	353.985	1310.734
		392.599	364.008	1102.824
119,600	7.5 (43)	392.190	378.537	735.454
		391.042	376.355	701.548
		391.055	385.051	667.599

References

1. Pontes, K. V.; Maciel, R.; Embiruçu, M. J Appl Polym Sci 2008, 109, 2176.
2. Pontes, K. V.; Maciel, R.; Embiruçu, M.; Hartwich, A.; Marquardt, W. AIChE J 2008, 54, 2346.
3. Embiruçu, M.; Pontes, K.; Lima, E. L.; Pinto, J. C. Macromol React Eng 2008, 2, 161.
4. Harismiadis, V. I.; Tassios, D. P. Ind Eng Chem Res 1996, 35, 4667.
5. Fontes, C. H. O.; Embiruçu, M. Comput Chem Eng 2001, 25, 191.
6. Costa, G. M. N.; Guerrieri, Y.; Kislansky, S.; Pessoa, F. L. P.; de Melo, S. A. B. V.; Embiruçu, M. Ind Eng Chem Res 2009, 48, 8613.
7. Embiruçu, M.; Fontes, C. Chem Eng Sci 2006, 61, 5754.
8. Tumakaka, F.; Prikhodko, I. V.; Sadowski, G. Fluid Phase Equilib 2007, 260, 98.
9. Abbas, S.; Mukherjee, R.; De, S.; Ganguly, S. Chem Eng Process 2004, 43, 1449.
10. Pan, C.; Radoz, M. Fluid Phase Equilib 1999, 155, 57.
11. Poling, B.; Prausnitz, J.; O'Connell, J. The Properties of Gases and Liquids, 5th ed., McGraw-Hill: New York, 2001.
12. Boukouvalas, C.; Spiliots, N.; Coutsikos, P.; Tzouvaras, N.; Tassios, D. P. Fluid Phase Equilib 1994, 92, 75.
13. Wong, D. S. H.; Sandler, S. I. AIChE J 1992, 38, 671.

14. Soave, G. Chem Eng Sci 1972, 27, 1197.
15. Costa, G. M. N.; Dias, T.; Cardoso, M.; Guerrieri, Y.; Pessoa, F. L. P.; de Melo, S. A. B. V.; Embiruçu, M. Fluid Phase Equilib 2008, 267, 140.
16. Henrici, P. Elements of Numerical Analysis; Wiley: New York, 1964.
17. Ralston, A.; Rabinowitz, P. A First Course in Numerical Analysis, 2nd ed.; McGraw-Hill: New York, 1978.
18. Atkinson, K. E. An Introduction to Numerical Analysis, 2nd ed.; Wiley: New York, 1989.
19. Stoer, J.; Bulirsch, R. Introduction to Numerical Analysis, 3rd ed.; Springer-Verlag: New York, 2002.
20. Gross, J.; Sadowski, G. Ind Eng Chem Res 2001, 40, 1244.
21. Gross, J.; Sadowski, G. Ind Eng Chem Res 2002, 41, 5510.
22. Bogdanic, G.; Vidal, J. Fluid Phase Equilib 2000, 173, 241.
23. Richards, R. B. Trans Faraday Soc 1946, 42, 10.
24. Nakajima, A.; Fujiwara, H.; Hamada, F. J Polym Sci Part A-1: Polym Chem 1966, 4, 507.
25. Kim, S. S.; Lloyd, D. R. Polymer 1992, 33, 1036.
26. Nakajima, A.; Fujiwara, H. J Polym Sci Part A-1: Polym Chem 1968, 6, 723.
27. Agarwal, R.; Prasad, D.; Maity, S.; Gayen, K.; Ganguly, S. J Chem Eng Jpn 2004, 37, 1427.
28. Gregorowicz, J. J. Supercrit Fluids 2007, 43, 357.
29. Condo, P. D., Jr.; Colman, E. J.; Ehrlich, P. Macromolecules 1992, 25, 750.
30. Zhang, W.; Dindar, C.; Bayraktar, Z.; Kiran, E. J Appl Polym Sci 2003, 89, 2201.
31. Van Krevelen, D. W. Properties of Polymers, 3rd ed.; Elsevier Scientific: Amsterdam, 1990.
32. Kontogeorgis, G.; Harismiadis, V. I.; Fredeslund, A.; Tassios, D. P. Fluid Phase Equilib 1994, 96, 65.
33. Elbro, H. S.; Fredesnlund, A.; Rasmussen, P. Ind Eng Chem Res 1991, 30, 2576.
34. Bondi, A. Physical Properties of Molecular Crystals, Liquids and Glasses; Wiley: New York, 1968.
35. Nelder, J. A.; Mead, R. Comput J. 1964, 7, 308.